Parameters to be considered for the development of highly photoactive TiO$_2$ layers on aluminium substrates by RF magnetron sputtering for treating polluted air

S. Suárez [a],[*], J. Pacha [a], S. Fernández [b], M.B. Gómez-Mancebo [c], F.J. Sánchez [d], C. Martínez [a], B. Sánchez [a]

[a] *FOTOAIR Unit, Avda. Complutense 40, 28040 Madrid, Spain*
[b] *Photovoltaic Unit, Avda. Complutense 40, 28040 Madrid, Spain*
[c] *Chemistry Division, Avda. Complutense 40, 28040 Madrid, Spain*
[d] *Fusion Technology Division, Avda. Complutense 40, 28040 Madrid, Spain*

ARTICLE INFO

ABSTRACT

In this study, photoactive titanium dioxide films deposited on aluminium substrates using Radio-Frecquency (RF) magnetron sputtering have been developed, with the goal of advancing this technology for indoor air treatment. With this goal in mind, the influence of deposition parameters, namely post annealed heat treatment, working pressure and deposition time, on the physico-chemical properties of the layers has been studied. Photocatalytic efficiency for trichloroethylene degradation in gas phase, and self-cleaning performance of the developed materials have been evaluated. Samples have been thoroughly examined using different techniques (SAXRD, UV-Vis, SEM-EDX, contact angle, profilometry, hardness, among others) in order to determine the structural-photocatalytic relationship. The findings indicate that high-temperature annealing promotes the diffusion of alumina, copper and iron ions towards the surface of the samples resulting in the formation of aluminium alloys. These alloyed species can act as recombination centres adversely affecting the photocatalytic activity. The sputtering pressure also affects the nature of the titanium phases formed during the sputtering. Increasing the thickness of the TiO$_2$ layer leads to rougher surfaces with TiO$_2$-anatase as the predominant crystal phase. Annealing temperatures of 350 °C, argon pressures between 0.8 and 1.0 Pa, and TiO$_2$ layer thickness of ca. 110 nm are the optimal conditions to prepare well-adhered TiO$_2$ layers with high photocatalytic performance. UV-A photoinduced superhydrophilicity phenomena was observed for all TiO$_2$/Al materials.

1. Introduction

The population living in developed countries spends more than 90% of their time indoors [1]. The concentration of pollutants in indoor air can be between two and five times higher than outdoors [2]. Thus, improving indoor air quality is essential to ensuring the health of the population [3]. Volatile Organic Compounds (VOCs), particles and microorganisms, are the main pollutants found in indoor air [4]. VOCs are widely found as ingredients of typical household products such as paints, varnishes and waxes [5]. VOCs include a variety of chemicals, some of which may have short- and long-term detrimental health effects (EPA 2017) [6,7]. These pollutants can produce important damage to the respiratory system and chronic diseases, with some pollutants being identified as carcinogenic substances [4].

Photocatalysis is a well-stabilised Advanced Oxidation Process (AOP), widely employed to control and reduce the concentration pollutants [8]. In a photocatalytic process, electron-hole pairs are produced in a semiconductor, resulting in oxidation and reduction reactions. OH$^\bullet$ and O$_2^\bullet$ radicals are responsible for the oxidation of the pollutants. Due to its high photoactivity, photochemical stability, low cost, and availability, TiO$_2$ is the benchmark commercial photocatalyst [9]. Despite the extensive research in the field of developing alternative photocatalytic materials, the commercial use of photocatalytic systems is still focussed on titanium oxide-based materials [10].

The use of immobilised photocatalysts is a fundamental requirement for air treatment decontamination units [11]. Thus, one of the main

---

Table 1
Samples prepared by RF magnetron sputtering.

Sample	Temperature (°C)	Pressure (Pa)	Time (min)	Thickness* (nm)	Ea (eV)	TiO$_2$ size (nm)	R$_a$** (nm)
Al	–	–	–	–	–	–	541
TiO$_2$/Al-0	as-dep.	1.0	240	179 ± 6	3.52		574
TiO$_2$/Al-1	350	1.0	240	155 ± 13	3.60	14	1762
TiO$_2$/Al-2	500	1.0	240	140 ± 7	3.70	13	986
TiO$_2$/Al-3	350	0.5	90	90 ± 10	3.75	11	1135
TiO$_2$/Al-4	350	0.8	120	99 ± 15	3.70	12	1302
TiO$_2$/Al-5	350	1.3	180	80 ± 9	3.75	12	1762
TiO$_2$/Al-6	350	1.0	70	40 ± 9	3.70	10	761
TiO$_2$/Al-7	350	1.0	170	111 ± 21	3.74	10	1448
TiO$_2$/Al-8	350	1.0	348	246 ± 30	3.58	10	2443
TiO$_2$/Al-9	350	1.0	510	412 ± 11	3.25	12	5884

*layer thickness was measured on Corning glass substrate (CG); **R$_a$ values were obtained on Al-based materials.

issues clearly identified for practical applications is the proper anchoring of the semiconductor layer onto the substrate to avoid the release of TiO$_2$ nanoparticles into air during operation. The final immobilised materials should be placed into decontamination units suitable for the treatment of a large volume of gases with low residence time. Glass and organic polymers are two of the most commonly used substrates for anchoring TiO$_2$, each having its own differentiating characteristics [12,13]. Aluminium is an interesting substrate for designing photocatalytic devices, since it combines the main properties of glass and organic polymers. It is a resistant, light and easily shaped material with a low price. Moreover, it is a good reflector of light, allowing better use of photons when shaped materials such as monolithic or baffled structures are selected. The development of a photocatalytic unit, combined with a conventional High Efficiency Particulate Air (HEPA) filtering system could greatly improve air quality.

Several deposition techniques for preparing metal oxide layers have been reported. Chemical vapour deposition [14,15] electron beam deposition [16], sol-gel [17,18] or magnetron sputtering processes [19,20] are some of the most typical of such processes. The synthesis of TiO$_2$ sols, and the deposition of thin films by dip-coating process is one of the most common approaches used for the deposition of TiO$_2$ layers. Nevertheless, features such as the adhesion and homogeneity of the film over the metal substrate needs to be improved in order to avoid the release of TiO$_2$ nanoparticles to the gas phase. Magneton sputtering, a physical deposition technique, is used extensively for the preparation of high-quality commercial coatings such as transparent conductive oxides (front contact and transparent antireflective electrodes) for photovoltaic solar cells, glazing products, self-cleaning surfaces, pollution removing membranes, solar fuel production or optoelectronic components [21–23]. This process offers several advantages: it is an easy to scale-up and clean process, that allows the production of uniform well-adhered homogeneous and hardness films with high reproducibility [24,25]. Radio-Frequency (RF) magnetron sputtering allows the use of a wide range of targets, not only conductive materials as in the case of Direct-Current (DC). Moreover, the incorporation of additional gases such as O$_2$ is not required to produce the metal oxide phases. The use of magnetron sputtering for the deposition of TiO$_2$ films on glass or silicon-based substrates is well covered in the literature [26,27]. In part, this is because detailed characteristics of the materials is obtained relatively easily. However, the literature concerning the deposition of TiO$_2$ layers on metallic substrates is scarce [28,29]. The deposition of TiO$_2$ coatings could protect the substrate from oxidation processes and chemical attract [30].

Bearing in mind these considerations, the goal of our work is the development of highly photoactive materials based on TiO$_2$/Aluminium prepared by RF magnetron sputtering. The TiO$_2$ deposition parameters, including the post annealing temperatura, the sputtering working pressure and the deposition time a have been analysed. The influence of these conditions on the TiO$_2$ crystal phases, surface roughness, particles morphology and optical properties has also been studied. Photocatalytic

properties were analysed using trichloroethylene as a model organochloride compound, usually used as solvent. Moreover, the self-cleaning performance of the materials developed under UV-A irradiation, has been studied as well.

2. Experimental

2.1. Photocatalyst preparation

Commercial aluminium (Al) plates of 0.8 mm thickness (Puraltock 99.5-H24) were used. TiO$_2$ thin films were deposited on Al substrates by RF magnetron sputtering using a commercial UNIVEX 450B bi-chamber sputtering system with confocal geometry. For the photocatalytic activity measurements, samples of 2.5 cm × 7.5 cm surface were prepared. For characterization purposes, reference samples of 2.5 × 2.5 cm^2 based on aluminium and corning glass (CG) were prepared in the same batch. Four magnetrons were placed at around 0.15 m from the centre of the substrate. The 4-inch commercial ceramic target of TiO$_2$, with a purity of 99.995%, was obtained from Neyco (Vacuum & Materials). The pressure of the chamber was 0^{-5} Pa. During the process, the flow of Ar (99.999%) was controlled with a mass-flow controller. The films were deposited at room temperature, 150 W and a working pressure ranging from 0.5 to 1.3 Pa. In order to obtain different nominal TiO$_2$ layer thicknesses, the deposition time varied from 70 to 510 min. After the deposition of samples, an annealing treatment at 350 or 500 °C with a heating rate of 3 °C min^{-1} was carried out for 3 h. Table 1 shows the nomenclature of the samples prepared along with the different operating conditions.

2.2. Physicochemical characterization

The roughness of the surface and the thickness of the TiO$_2$ layer were measured using a Profilometer Bruker DektakXT with a diamond tip (2 μm radius) and a tip force of 5 mg. Data analysis was performed using a Vision64 software. The layer thickness values obtained by profilometry were measured using CG-based materials. In the case of surface roughness, the measurements were performed over the Al samples.

The scanning electron microscopy characterization was carried out in a JEOL JSM-7600 F equipped with an INCA detector for energy dispersive X-ray spectroscopy, EDX. Crystal structure identification studies were conducted with a Marlvern-PANalytical X′Pert PRO ultrafast detector small-angle X-ray diffractometer (SAXRD) with CuKα (λ = 0.154 nm). The mean crystallite size was estimated using Scherrer's equation. XRF measurement were performed with a Malvern-Panalytical Axios Wavelength Dispersive X-ray Fluorescence spectrometer.

The adhesion of the TiO$_2$ thin films to the aluminium substrate was tested by a tape test following the guides provided by the ASTM D3359–09 standard test. Diffuse Reflection Spectroscopy DRS UV–VIS measurements were performed on a Perkin Elmer Lambda 650 S UV–Vis spectrophotometer with a 60 mm integration sphere. UV-Vis absorption spectra of the samples were collected between 900 nm and 200 nm
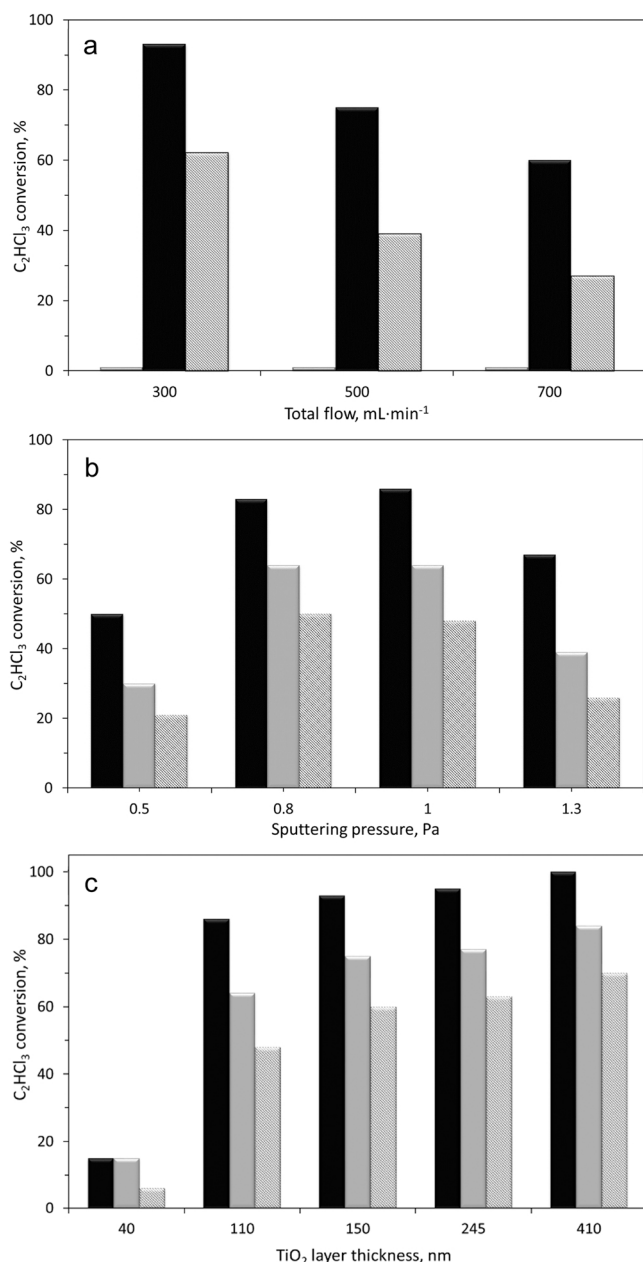
Fig. 1. Variation of the C_2HCl_3 conversion for TiO_2/Al samples with: a) annealed temperature: (▢) TiO_2/Al-0, (■) TiO_2/Al-1, (▨) TiO_2/Al-2, b) Sputtering pressure (TiO_2/Al-3, TiO_2/Al-4, TiO_2/Al-7, TiO_2/Al-5) and c) TiO_2 layer thickness (TiO_2/Al-6 to TiO_2/Al-9) at (■) 300 mL min^{-1}, (▢) 500 mL min^{-1}, (▨) 700 mL min^{-1}.

wavelengths with 4 nm steps. F(R) function was calculated according to equation: $F(R) = \left(\frac{1-R_\infty^2}{2R_\infty}\right)$ where R_∞ is the reflectance of the sample [29]. Band edge energy was calculated according the Tauc plot, representing $(F(R_\infty)E)^{1/2}$ vs. the energy of the exciting light (hν) in the region between 3.0 and 4.0 eV, considering forbidden indirect transitions ($\gamma = 2$) [31]. Raman spectra were acquired by using a Horiba LabRam HR evolution spectrometer (Jobin Yvon Technology). The 532 nm laser beam was focused onto the sample through the 5x objective of an Olympus BX41 microscope.

Surface hydrophilicity-hydrophobicity was measured by water contact angle (WCA) measurements with a Krüss DSA Drop Shape Analyzer. A volume of 3 µL of distilled water was deposited on the surface of the sample using an automated micro-injector at a velocity of 120 µL min^{-1}

. The influence of the UV-A on the contact angle was studied using two UV-A Sylvania 8 W low power lamps after irradiating the samples for 30 and 60 min. Analyses were performed with at least two samples. The values presented in the article correspond to the arithmetic mean.

2.3. Photocatalytic activity tests

The photocatalytic oxidation reaction of trichloroethylene (C_2HCl_3) in air was carried out in a stainless-steel continuous flow flat photoreactor (120 mm × 50 mm × 10 mm). The samples were irradiated by two 8 W Sylvania UV-A lamps with a maximum emission at 365 nm wavelength and light intensity of 6 W cm^2. The pollutant feeding was performed using a gas cylinder (C_2HCl_3/N_2 Air Liquide) with a controlled composition of trichloroethylene (500 ppm). C_2HCl_3 was mixed with compressed air free of water and CO_2. The concentration of C_2HCl_3 was set at 25 ppm and the total flow between 300 and 700 mL min^{-1}. The flow rate was controlled using electronic mass flow controllers. The gas composition was monitored during the experiments by using an FTIR Thermo-Nicolet 5700 spectrometer [32].

The evolution of the concentration of C_2HCl_3 and reaction products was obtained through the integration of the characteristic IR band for each component. The conversion of the organochloride compound ($X_{C_2HCl_3}$) was calculated according to $X_{C_2HCl_3} = \frac{C_2HCl_{3\,inlet} - C_2HCl_{3\,outlet}}{C_2HCl_{3\,inlet}} \cdot 100$ where $C_2HCl_{3\,inlet}$ and $C_2HCl_{3\,outlet}$ are the trichloroethyle concentrations at the reactor inlet and outlet.

3. Results and discussion

The most relevant RF magnetron sputtering deposition parameters for the preparation of the TiO_2/Al films are shown in Table 1. The effect of the post-annealed temperature, working pressure, and deposition time on the physico-chemical and photocatalytic performance of the samples was analysed. The thickness of the TiO_2 film and the roughness values - expressed as arithmetic mean roughness (Ra) - as determined by profilometry, as well as the band edge energy, are given in Table 1.

3.1. Effect of the post-deposition heat treatment temperature

First, the effect of the annealing temperature of the TiO_2 layers deposited on aluminium foils was studied. The photooxidation of C_2HCl_3 over the as-deposited samples and for those annealed at 350 °C and 500 °C and at different gas flow rates was studied. The results obtained with the samples prepared using the same deposition conditions are shown in Fig. 1a. As can be seen, the annealing temperature has an important effect on the photocatalytic activity of the TiO_2/Al samples. Thus, the non-annealed sample (TiO_2/Al-0) is almost inactive as regards the photodegradation of the organochloride compound irrespective of the gas flow. The sample annealed at 350 °C (TiO_2/Al-1) yielded a high C_2HCl_3 conversion at all of the flow rates studied in this work, reaching conversions higher than 90% at 300 mL min^{-1}, but declining at higher flow rates. However, the activity of the sample annealed at 500 °C (TiO_2/Al-2) is lower than that of (TiO_2/Al-1) at all flow rates, reaching C_2HCl_3 conversion values around 65% at 300 mL min^{-1}. As expected, the photocatalytic efficiency decreased with the increasing gas flow, since the contact time is reduced. In order to understand the effect of the temperature used for the annealing treatment on the physico-chemical properties of the TiO_2/Al samples, different parameters were studied. Fig. 2a shows the SAXRD diffractograms of the samples obtained at each annealing temperature. The non-annealed as-deposited layer (TiO_2/Al-0) shows the characteristic diffraction fingerprints for aluminium with the peaks at 38.5° and 44.7° being ascribed to the (111) and (200) planes, respectively (ICDD 03–065–2869). A closer inspection of the diffractogram for TiO_2/Al-0 reveals low intense peaks at 37.7° and 43.1°, indicative of the presence of an aluminium oxide phase (ICDD 01–077–2135). The characteristic diffraction pattern of TiO_2-anatase is

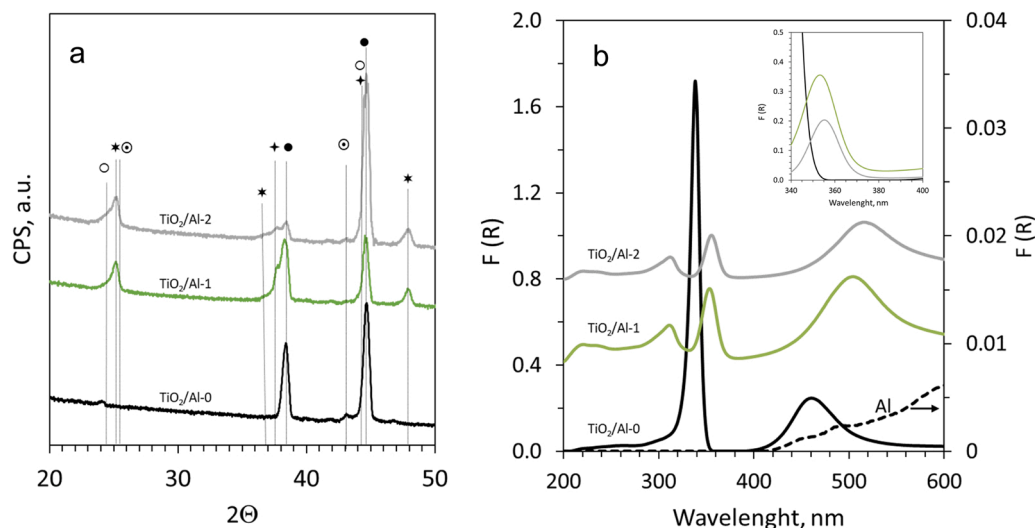**Fig. 2.** a) SAXRD diffractograms and b) DRS UV-Vis spectra for TiO$_2$/Al samples annealed at different temperature. ($*$) TiO$_2$-anatase, ($\bullet$) aluminium, ($\bigcirc$) Al/Cu or Al/Fe, ($\blacklozenge$) AlTi, ($\odot$) Al$_2$O$_3$.
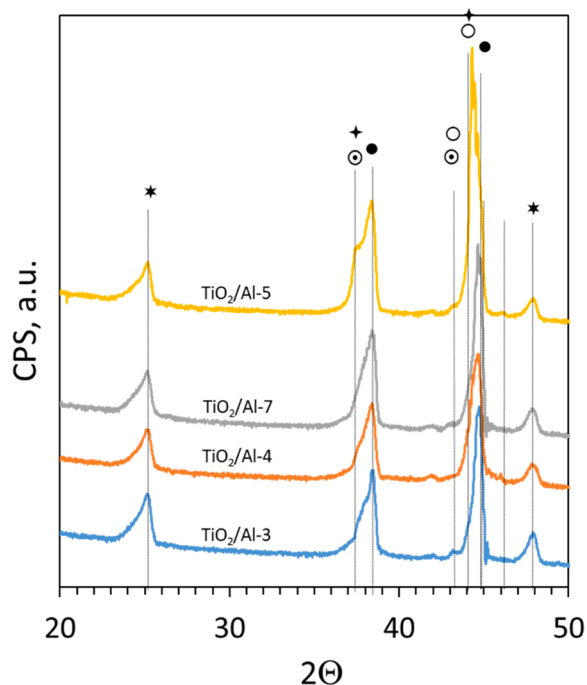
Fig. 3. SAXRD diffractograms for TiO$_2$/Al samples prepared at different working pressure. ($*$) TiO$_2$-anatase, ($\bullet$) aluminium, ($\bigcirc$) Al/Cu or Al/Fe, ($\blacklozenge$) Al/Ti, ($\odot$) Al$_2$O$_3$.

visible for samples annealed at 350 °C and 500 °C (ICDS 98–009–4633), showing the characteristic reflections at 25.4° and 48.0°, with the former peak corresponding to the (101) planes of TiO$_2$-anatase phase. Peaks ascribed to other TiO$_2$ phases (rutile or brookite) were not detected. These results were confirmed by Raman spectroscopy. As expected, metallic aluminum substrate does not show any Raman features in the region studied. The Raman spectrum for TiO$_2$/Al-0 (as deposited, without thermal treatment) also fails to show Raman peaks, since no crystalline TiO$_2$ phase was detected according to XRD. The spectra for samples annealed at 350 and 500 °C display peaks at 134, 382, 500, and 618 cm^{-1}, characteristics of the Eg, B1g, A1g and Eg Raman active modes of TiO$_2$-anatase [33]. Fig. 1SI shows the band at 134 cm^{-1} for the samples treated 350 and 500 °C.

Noticeably, the peaks centred at 38.5° in the diffractograms for TiO$_2$/Al-2 and TiO$_2$/Al-3 broaden and unfold into at least two contributions in the range between 37° and 39°. This effect, i.e., the appearance of further diffraction peaks within this 2θ region, suggests the presence of a titanium aluminide phase (ICDS 98–008–0835), with a characteristic diffraction peak at 37.5°. Although the alumina phase contributes at this angle, the intensity of the signal is negligible. In addition, a slight contribution of the TiO$_2$-anatase phase with a peak at 37.0° can be appreciated. This effect can be also observed for the peak at 45.0°, which presents a single, symmetric peak in the diffractograms of TiO$_2$/Al-0, unfolding into 2–3 well-defined peaks for the samples annealed at 350 and 500 °C. Along with the aluminium phase, the presence of iron-aluminium and/or copper-aluminium alloyed phases (ICDS 98–007–7248, 00–045–0982) cannot be ruled out. The identification of these phases is not easy, since their diffraction peaks overlap with those of titanium aluminide alloy. It is important to bear in mind that this peak considerably increases in intensity for the TiO$_2$/Al-2 sample annealed at 500 °C. On the contrary, the intensity of the diffraction planes in the region between 37° and 38° decreases. Considering the nature of the SAXRD analysis, it is difficult to establish a proper correlation between the intensity of the diffraction peaks and the concentration of the crystalline phases. Nevertheless, the results presented here suggest that the formation of aluminium alloyed phases of iron, copper or titanium is favoured by higher annealing temperature. A careful inspection of the Raman spectra reveals how the position of the Raman band shifts with the annealing temperature (Fig. 1 SI). Thus, the peak for TiO$_2$/Al-1 (350 °C) is centered at 134 cm^{-1}, shifting to 132 cm^{-1} in the spectrum of TiO$_2$/Al-2 (500 °C). This shifting indicates that the annealing temperature affects the coordination of the titanium atoms with the oxygen ones. The composition of the aluminium plates was analysed by XRF. Aluminium is the main component with a 97 wt%, with Fe (0.54 wt%) and Cu (0.036 wt%) being the only other metallic elements detected. Aluminium ions can diffuse from the substrate to the TiO$_2$ layer acting as charge recombination centres. As a result, the photocatalytic activity of the TiO$_2$ layer decreases, as reported by Ho et al. [34]. It seems plausible that the formation of Cu- or Fe-Al alloys could favour the formation recombination centres, hence decreasing the photocatalytic performance. This line of reasoning explains the observed decrease of the photocatalytic activity of the sample annealed at 500 °C (TiO$_2$/Al-2).

To study the influence of the calcination temperature on the optical properties of TiO$_2$ films, the DR UV-Vis spectra were analysed. In Fig. 2b the Kubelka-Munk spectra for as-deposited and annealed samples are shown. The spectrum for TiO$_2$/Al-0 shows bands centred at 338 nm and
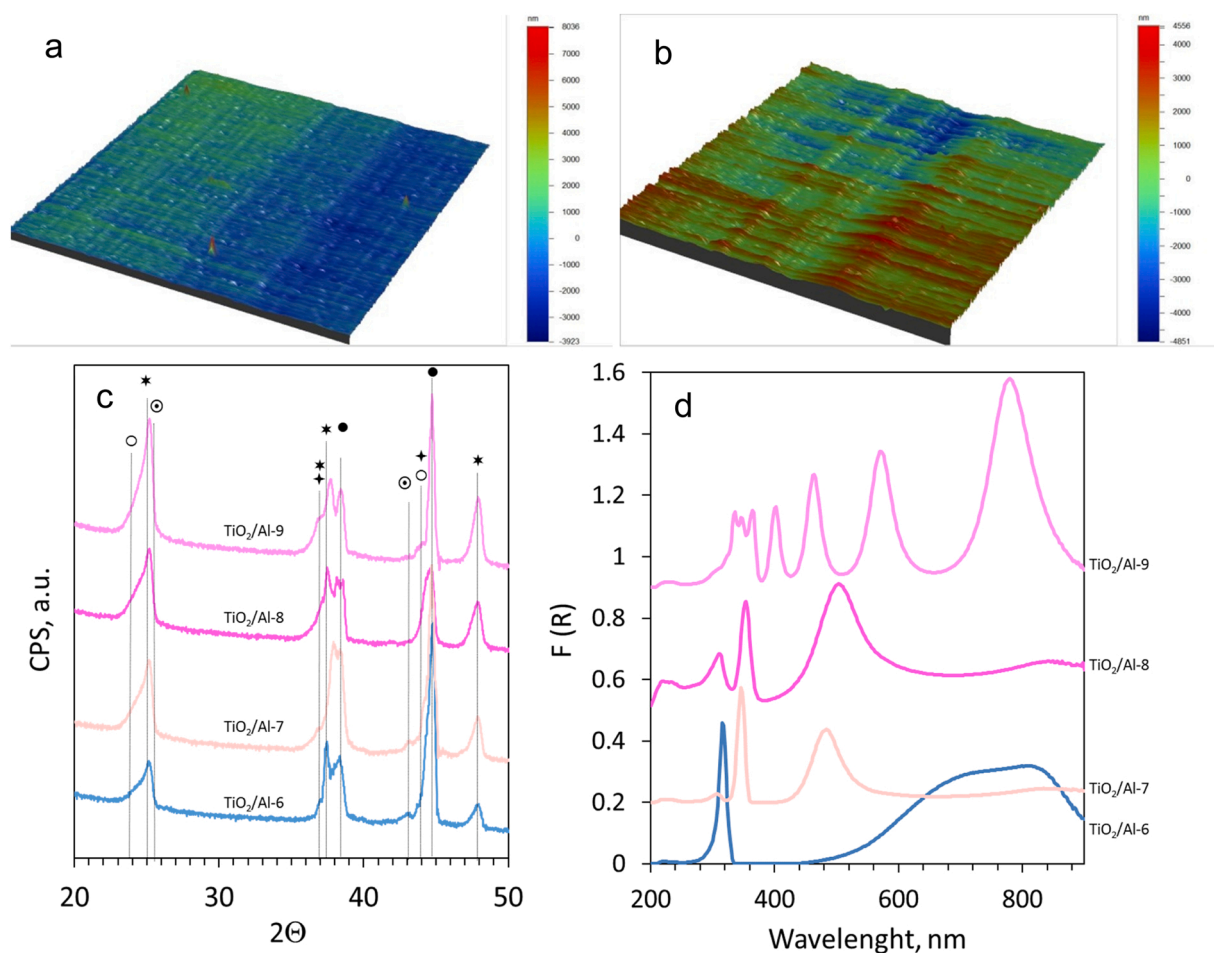
Fig. 4. Images of the surface roughness for a) TiO₂/Al-6 and b) TiO₂/Al-8. Effect of TiO₂ layer thickness by c) SAXRD diffractograms and d) DRS UV-Vis spectra for TiO₂/Al samples. (✱) TiO₂-anatase, (•) aluminium, (◯) Al/Cu or Al/Fe, (✦) Al/Ti, (◉) Al₂O₃.

458 nm. These bands shift to 356 nm and 518 nm, respectively, in the spectra of the annealed samples. Zhu et al. reported a similar trend for TiO₂/stainless steel materials [35]. The redshift probably accounts for the aluminium alloys detected by XRD. The absorption of UV light mainly results from the promotion of 3d electrons in the titania crystal field. Since the diffusion of these elements increased as the annealing temperature rose, the change in the optical properties of the coating becames more pronounced as the annealing temperature increase. The band edge energy moves from 3.5 eV for TiO₂/Al-1 with an amorphous TiO₂ phase to 3.3 eV for TiO₂/Al-1 sample. This adsorption energy is characteristic of TiO₂-anatase. The changes of the band in the region between 340 and 380 nm and in the adsorption edge for annealed materials (Fig. 2b inlet) could be related not only to the changes in the aluminium alloys, but also to changes in the layer density [36,37].

According to profilometric measurements, the surface roughness (Ra) of TiO₂/Al-1 is greater than that of the Al substrate. Nevertheless, a notable reduction in roughness is observed for TiO₂/Al-2 (Table 1.), along with a slight decrease in TiO₂ layer thickness for the sample annealed at 500 °C. The Ra values decreased ca. 44% for TiO₂/Al-2. When the annealing temperature is raised, a densification of the TiO₂ layers occurs. This is another factor to be considered for the explanation of the drop in the photocatalytic activity observed for TiO₂-Al-500. The effect of the annealing treatment on the morphology of the TiO₂ particles was studied by SEM. As shown in Fig. 2 SI, the aluminium surface is covered by TiO₂ particles of ca. 12–14 nm, in good agreement with the SAXRD analysis. Grains can be better identified for annealed materials where the TiO₂ crystal phase is present. Moreover, cauliflower-like aggregates can be identified. The size of these aggregates goes from ca.

300 nm to near 1 μm. No significant differences in the size of the primary particles or in the mean crystal size of the particles obtained at different annealing temperatures were observed by SEM or SAXRD.

The results presented above suggest that changes in the nature of the phases present in the TiO₂ films by migration of cations from the substrate to the surface and the subsequent formation of aluminium alloys, along with TiO₂ layer densification and surface roughness are affected by the annealing temperature. According to these results, the calcination temperature selected for further studies was set to 350 °C.

3.2. Effect of the working pressure

The influence of the argon sputtering pressure on the photocatalytic properties of the samples was studied by varying the sputtering chamber pressure from 0.5 to 1.3 Pa. In order to keep the thickness of all layers the same at around ca. 100 nm, the deposition time for each sample was adjusted. Fig. 1b shows the results obtained for samples prepared at different argon pressures, treated at the temperature selected. The working pressure of sputtering influenced the photocatalytic performance of the materials obtained at the three gas flows studied. Maximum C₂HCl₃ conversions were obtained for the samples prepared at pressures of 0.8 and 1.0 Pa. C₂HCl₃ conversion decreases considerable for the samples prepared at 0.5 Pa or for those prepared at pressures above 1.0 Pa.

According to the Ra values shown in Table 1, the roughness of the surface increases linearly with the working pressure, with values ranging from ca. 1100 nm to 1800 nm for TiO₂/Al-3 and TiO₂/Al-5 respectively. This effect could positively impact the photocatalytic
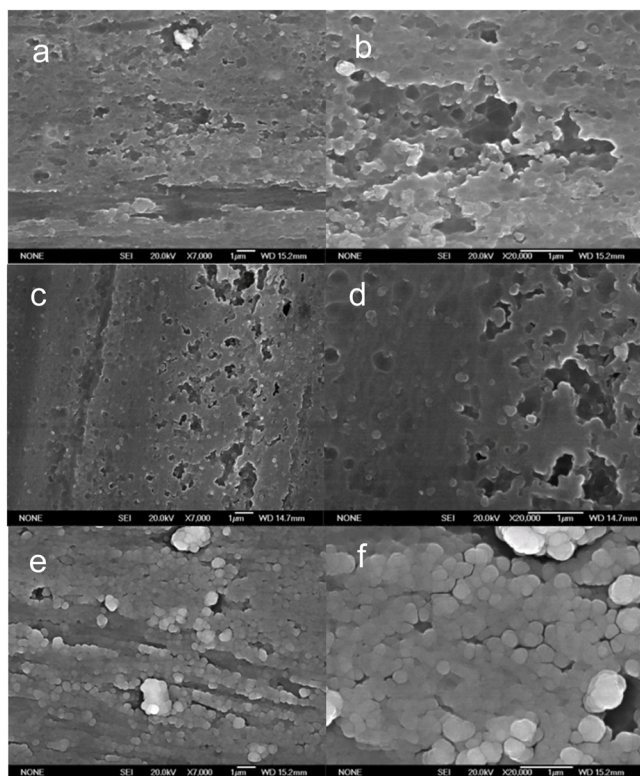
Fig. 5. SEM micrographs for TiO$_2$/Al samples with different TiO$_2$ layer thickness. a, b) TiO$_2$/Al-6, c, d) TiO$_2$/Al-7 y e, f) TiO$_2$/Al-9.

performance, due to the improvement in mass-transfer effects. Nevertheless, the maximum photocatalytic activity was observed for surface roughness values around 1300–1400 nm. Previous results in the literature reported the influence of the chamber pressure on layer compaction [38]. Thus, higher sputtering pressures result in less compact coatings. At high pressures the density of the gas increases, which increases the scattering of the sputtered particles. As a result, fewer particles successfully reach the substrate, resulting in a less dense film, i.e., fewer titanium sites per surface area. Nevertheless, the plateau observed in Fig. 1b, at working pressures between 0.8 and 1.0 Pa, indicates that other factors should be considered to understand the photocatalytic properties.

As shown in Fig. 3, all samples present the characteristic peak of TiO$_2$-anatase. The intensity and width of the peak centred at 25.4° is independent of the pressure at which the samples were prepared. It appears as if working pressure had no effect on the mean crystal size of the TiO$_2$ particles. The presence of an Al$_2$O$_3$ phase in all samples is responsible for the diffraction line at 43.1° observed in the diffractograms of all samples. As previously observed, the peak centred at ca. 45° unfolds into two contributions. This effect is clearly observed in the diffractogram of the TiO$_2$/Al-5 sample, in which the intensity of the peak increases, and a further contribution at 44.4° becomes noticeable. Moreover, two well-defined peaks at 37.5° and 38.4° can be clearly identified for this sample. The peaks centred at 44.4° and 37.5° can be attributed to a titanium aluminide phase, see Section 3.1 above. These results suggest that high argon pressures during sputtering promote the formation of a titanium aluminide phase. As also discussed above, this phase could have a negative effect on the photocatalytic performance of the materials. Other phases such as aluminium copper or aluminium iron phases could be also present on the samples; however, their presence is difficult to detect only by means SAXRD, since their characteristic reflections are close to those from titanium aluminide phases.

The optical properties of this series were also analysed (Fig. 3 SI). Samples prepared in the pressure range between $0.5 < P < 1.0$ Pa display similar spectra, with defined bands at 310 and 380 nm. The band located at 380 nm shows a red shift in the spectra of the samples prepared under high argon pressure. As previously explained, this could be related to the formation of aluminium alloys and their interaction with the titania atoms, prompted by high argon pressures. As for the sample prepared at low argon pressure, the lower surface roughness could be one of the factors for the low C$_2$HCl$_3$ conversion value obtained compared to samples prepared at 0.8–0.1 Pa. Band edge energy values (Table 1) of ca 3.7 eV were determined for all samples in the series. Some authors associate the increase of the band gap energy, compared to that of TiO$_2$ anatase, with the decrease of the number of oxygen vacancies [38,39].

SEM micrographs are shown in Fig. 4 SI at two magnifications. The presence of TiO$_2$ particles with a homogenous morphology is clearly observed. The presence of macrospores is evident for samples prepared at 1.0 Pa. This is not so evident for the sample prepared at 0.5 Pa. Moreover, the porous structure seems to change when the argon pressure increases to 1.3 Pa, with small pores being observed. In line with previous results, the presence of grains with a heterogeneous distribution is also observed [40]. It is important to notice that the TiO$_2$ layer mimics the shape and defects of the aluminium substrate, as if an epitaxial growth of the TiO$_2$ layer is produced. Lines or bands characteristics of the aluminium extrusion process can be noted in these micrographs.

The results obtained indicate that the pressure of argon during the sputtering has a strong effect on the composition of the coating, and as a consequence on their photocatalytic performance. Modifications in
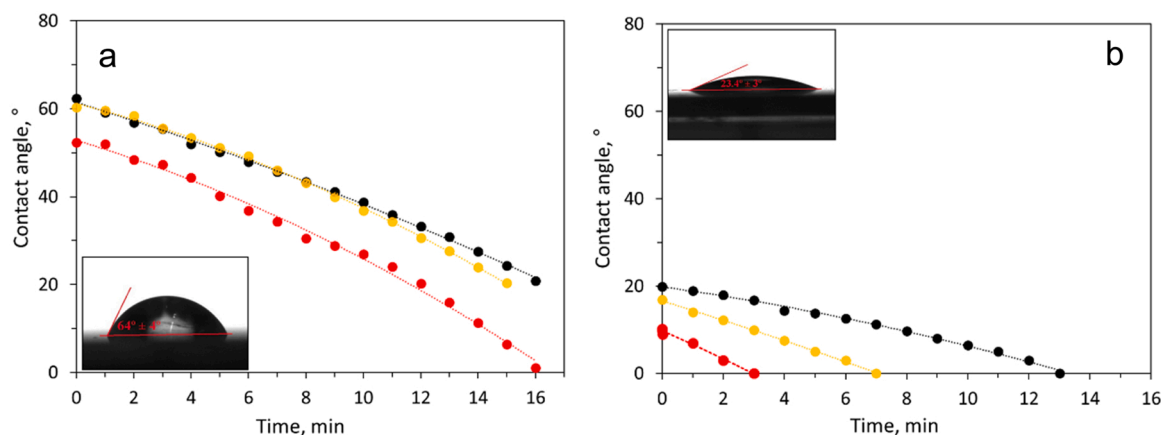

Fig. 6. Effect of the UV-A irradiation on the water contact angle for: a) aluminum substrate and b) TiO$_2$/Al-1 sample. (●) dark conditions (🟡) UV-A t = 0 min (🔴)UV-A t = 30 min.

surface roughness, optical properties and titanium crystal phases, fostering the formation of aluminium alloys at the surface were observed.

3.3. Effect of the deposition time

Finally, the effect of the deposition time, keeping constant the working pressure and the heat treatment temperature, was studied. The change of the deposition time leads to samples with different layer thicknesses (Table 1, samples from TiO_2/Al-6 to TiO_2/Al-9). Thus, TiO_2/Al samples with TiO_2 layer thickness from ca. 50–400 nm were obtained by varying the deposition times between 70 and 510 min. The photocatalytic activity results at different total gas flows are shown in Fig. 1c. A visible improvement of the photocatalytic performance was achieved when the layer thicknesses growths from 40 to 110 nm. Over this value, this trend is dampened and the effect on TiO_2 layer thicknesses is less pronounced. Thus, the maximum photocatalytic activity was obtained with TiO_2/Al-9, achieving values close to 100% for the sample with a TiO_2 layer thickness of 410 nm. The change of the titanium layer thickness between 110 and 410 nm only accounts to 15% increase of the C_2HCl_3 conversion. Nevertheless, the time for deposition is notably increased.

The increase of the thickness of the titania layer has an important effect on the surface roughness, as can be seen in Table 1. Representative images are shown in Fig. 4a), b) for TiO_2/Al-6 and TiO_2/Al-8. The Ra values increase from 761 to 5884 nm as a result of the TiO_2 layer thickness. As explained above, the extrusion process of the aluminium plates confers a characteristic surface morphology, leading to the appearance of lines and defects. The growth of the TiO_2 layer tends to mimic the aluminium surface. This effect becomes more noticeable for the samples with high layer thickness.

Changes in the crystalline phases and in the optical properties with coating thickness were analysed (Figs. 4c and 4d). The increase in the intensity of TiO_2 peaks at 25° from the TiO_2-anatase phase, with the layer thickness observed. The mean crystal size of the TiO_2 particles is not affected by the deposition time. Along with aluminium and alumina crystal phases, certain aluminium alloy phases (with Cu and Fe), were again detected. The Cu or Fe and Ti aluminium alloy phases can be better appreciated in the samples with the thinnest TiO_2 layers (TiO_2/Al-6 and TiO_2/Al-7). It is interesting to highlight the noticeably small contribution of the titanium aluminide phase for the material prepared at high deposition times, with a characteristic contribution at 44°. The intensity of this peak is strongly reduced for samples with 250 and 450 nm TiO_2 layer thicknesses, aluminium and TiO_2-anatase being the predominant crystal phases identified.

Regarding the optical properties, the thickness of the TiO_2 layer has a strong influence in the number of maxima and minima observed in the spectra. As expected, the optical interference increased due to the effect of layer thickness. Band edge energy values were calculated, moving from ca. 3.7–3.2 for TiO_2/Al-6 to TiO_2/Al-9, respectively. As explained above, the primary determinants of the higher binding energy values at low TiO_2 layer thicknesses seems to be the different aluminium-alloyed species and titania oxygen vacancies present. Thick layer of around ca. 410 nm, display binding energy values around 3.2 eV, the characteristic value for TiO_2-anatase.

The morphological features of the TiO_2 coatings were analysed by SEM microscopy. Fig. 5 shows representative micrographs of the samples; those prepared with low coating thicknesses display a more porous structure than the samples obtained during longer sputtering times. Thus, the surface TiO_2/Al-9 is quite homogeneous. The presence of aggregates with mean sizes of 300–400 nm were also detected. In spite of the excellent photocatalytic properties of TiO_2/Al-9, sputtering deposition time will increase the economic cost associated to the preparation process. Thus, samples with layer thickness in the range between 100 and 250 nm, requiring lower deposition times, are more suitable from an economic point of view.

The adherence and hardness of the TiO_2 coating on the aluminium substrates are among the main advantages of coatings prepared by RF magnetron sputtering. The adherence of the TiO_2 layers was analysed according to the ASTM D3359–09 standard test. All samples reached the maximum 5B score according to this standard, demonstrating the great adhesion of the TiO_2 coating prepared by this RF magnetron sputtering.

The hydrophilic or hydrophobic character of the surface is a highly relevant property for self-cleaning applications. The variation of the water contact angle (WCA) with time for the aluminium substrate and TiO_2/Al-1, under dark conditions and in presence of UV-A light is shown in Fig. 6a and Fig. 6b, respectively. The aluminium substrate has a WCA of $64° \pm 4°$, which remains almost the same for the irradiated samples. The decrease of the WCA values observed with the irradiation time was attributed to the thermal effect produced by the UV-A irradiation source. The incorporation of the TiO_2 coating by sputtering leads to a strong decrease in WCA values, indicative of the development of a more hydrophilic surface, showing WCA values ca. $20° \pm 3°$ Fig. 6b. This value further decreases to values characteristic of superhydrophilic surfaces ($\theta < 10°$) for the TiO_2/Al samples obtained after 30 min UV-A irradiation. All TiO_2/Al materials prepared by RF magnetron sputtering presented this property, irrespectively of the calcination temperature.

4. Conclusions

The results obtained in this work reveal that highly photoactive materials based on TiO_2 layers deposited on aluminium substrates can be prepared by RF magnetron sputtering using a TiO_2 ceramic target. Annealing temperature, deposition time and working pressure are important parameters to be considered during TiO_2 sputtering, since they inform about the physicochemical properties of the materials obtained and hence their photocatalytic performance. The operating conditions and the nature of the substrate components can affect the formation of foreign aluminium alloys, optical properties and surface roughness. However, the morphology of the primary titanium particles or grain size seems not to be greatly influenced by the sputtering conditions. The porous structure of the coating appears to be more related to the surface nature of the aluminium substrate. This technology is suitable for the preparation of TiO_2 well adhered layers over large surfaces with different shapes, being especially suitable for applications in photocatalytic decontamination units for indoor air treatment. Experiments are currently being carried out with these materials on a large scale for the treatment of indoor air. TiO_2/Al materials present UV-A induce superhydrophilicity, opening its application window to other sectors.

CRediT authorship contribution statement

SS conceptualising and supervising the work, interpretation of the results, literature research, manuscript writing and review; JP photocatalytic activity experiments, characterization of samples, literature research; SF conceptualising the work, literature search, samples preparation, characterizacion and interpretation of the results; MBG SADRX and XRF analysis and interpretation of the results, revision of the manuscript; FJS profilometric measurements; CM analysis of the photocatalytic activity experiments and literature search; BS conceptualising the work and raise funding.

Declaration of Competing Interest

The authors declare that they have no known competing financial interests or personal relationships that could have appeared to influence the work reported in this paper.

Data availability

No data was used for the research described in the article.

Acknowledgments

Appendix A. Supporting information

Supplementary data associated with this article can be found in the online version at doi:10.1016/j.cattod.2022.12.001.

References

[1] J.D. Spengler, Y.K. Sexton, Science vol. 221 (nº 4605) (1983) 9–17.
[2] U.S. Environmental Protection Agency. 1987. The total exposure assessment methodology (TEAM) study: Summary and analysis. EPA/600/6–87/002a. Washington, DC.
[3] K.W. Tham, Energy Build. 130 (2016) 637–650.
[4] V.V. Tran, D. Park, Y.-C. Lee, Int. J. Environ. Res. Public. Health 17–8 (2020) 2927.
[5] L. Lucattini, G. Poma, A. Covaci, J. de Boer, M.H. Lamoree, P.E. Leonards, Chemosphere 201 (2018) 466–482.
[6] Air quality in Europe— 2016 report No 28/2016 ISBN 978–92-9213–847-9 (EEA).
[7] EPA, Volatile Organic Compounds' Impact on Indoor Air Quality, in: ⟨www.epa.gov⟩, 2017.
[8] Y. Boyjoo, H. Sun, J. Liu, V.K. Pareek, S. Wang, Chem. Eng. J. 310 (2) (2017) 537–559.
[9] O. Carp, C.L. Huisman, A. Reller, Prog. Solid State Chem. 32 (2004) 33–177.
[10] M. Muscetta, D. Russo, Photocatalytic applications in wastewater and air treatment: a patent review (2010–2020), Catalysts 11 (2021) 834.
[11] S. Suárez, Chap. 12. Immobilised Photocatalysts, in Design of Advanced Photocatalytic Materials for Energy and Environmental Applications Eds. J. Coronado, F. Fresno, M.D. Hernandez-Alonso, R. Portela. ISBN: 978–1-4471–5061-9.
[12] N. Miranda-García, S. Suárez, B. Sánchez, J.M. Coronado, S. Malato, M. I. Maldonado, Appl. Catal. B 103 (2011) 294–301.
[13] R. Portela, B. Sanchez, J.M. Coronado, R. Candal, S. Suarez, Catal. Today 129 (2007) 223–230.
[14] K.L. Choy, Prog. Mater. Sci. 48 (2003) 57–170.
[15] C.Y. Chang, Y.H. Hsieh, Y.Y. Chen, Int. J. Photo 6 (2012) 1–6. ID 576089.
[16] A. Fouda, K. Hazu, T. Nakayama, S.F. Chichibu, Phys. Stat. Sol. C. 8 (2011) 534–536.
[17] R.M. Cámara, E. Crespo, R. Portela, S. Suárez, L. Bautista, F. Gutiérrez-Martín, B. Sánchez, Catal. Today 230 (2014) 145–151.
[18] M. ernasik, M. Radecka, M. Rekas, Sloma, Appl. Surf. Sci. 65–66 (1993) 240–245.
[19] P.J. Kelly, R.D. Arnell, Vacuum 56 (2000) 159–172.
[20] L. Li, Z. Wu, Y. Ju, C. Chen, Energy Procedia 12 (2011) 456–461.
[21] S. Swann, Magnetron sputtering, Phys. Technol. 19 (1988) 67–75.
[22] P.J. Kelly, G.T. West, M. Ratova, L. Fisher, S. Ostovarpour, J. Verran, Molecules 19 (2014) 16327–16348.
[23] F. Fresno, P. Brasa, E. Alfonso González, C. Guillén, J. Trigo, J. Herrero, L. Collado, V. de la Peña O'Shea, Appl. Catal. B 224 (2018) 912–918.
[24] P.B. Nair, V.B. Justinvictor, G.P. Daniel, K. Joy, K.C. James Raju, D. Devraj Kumar, P.V. Thomas, Pro. Nat. Sci. -Mater. 24 (2014) 218–225.
[25] K. Elmer, J. Phys. D: Appl. Phys. 33 (2000) R17.
[26] C. Guillén, J. Montero, J. Herrero, J. Mater. Sci. 49 (2014) 5035–5042.
[27] H. Najafi, A. Karimi, D. Alexander, P. Dessarzin, M. Morstein, Thin Solid Films 549 (2013) 224–231.
[28] S. Daviðsdóttir, S. Canulescu, K. Dirscherl, J. Schou, R. Ambat, Surf. Coat. Technol. 216 (2013) 35–45.
[29] S. Daviðsdóttira, R. Shabadib, A. Catalin Galcac, I.H. Andersend, K. Dirscherle, R. Ambat, Appl. Surf. Sci. 313 (2014) 677–686.
[30] M. Guglielmi, J. Sol-Gel, Sci. Technol. Vol. 8 (No. 1–3) (1997) 443–449.
[31] J. Tauc, Mater. Res. Bull. 5 (1970) 721–729.
[32] I. Jansson, S. Suárez, F.J. Garcia-Garcia, B. Sánchez, Appl. Catal. B 178 (2015) 100–107.
[33] W. Su, J. Zhang, Z. Feng, T. Chen, P. Ying, C. Li, J. Phy. Chem. C. 112 (2008) 7710–7716.
[34] W. Ho, J.C. Yu, S. Lee, Appl. Catal. B 73 (2007) 135–143.
[35] Y. Zhu, L. Zhang, L. Wang, Y. Fu, L. Cao, J. Mater. Chem. 11 (2001) 1864–1868.
[36] G. Kenanakis, D. Bemardou, A. Dalamagkas, N. Katsarakis, Catal. Today 240 (2015) 146–152.
[37] T. Tański, W. Matysiak, D. Kosmalska, A. Lubos, 66-2, Bull. Pol. Acad. Sci. Tech. Sci. (2018), https://doi.org/10.24425/119069.
[38] K. Eufinger, E.N. Janssen, H. Poelman, D. Poelman, R. De Gryse, G.B. Marin, Thin Solid Films 515 (2006) 425–429.
[39] M. Acosta, D. González, I. Riech, Thin Solid Films 517 (2009) 5442.
[40] P.B. Nair, V.B. Justinvictor, G.P. Daniel, K. Joy, V. Ramakrishnan, P.V. Thomas, Appl. Surf. Sci. 257 (2011) 10869–10875.